SUPPORTING INFORMATION

Interface engineering induced hierarchical NiCo/V_2O_3/C Schottky heterojunction catalyst for large-current-density hydrogen evolution reaction

Danyang Li[a,b], Jingkai Wang[a,b], Shenghui Wang[a], Bingxian Chu[a], Rongyao Li[a], Bin Li[a,b], Lihui Dong[a,b], Minguang Fan[a,b*], and Zhengjun Chen[a,*]

[a]Guangxi Key Laboratory of Electrochemical Energy Materials, Guangxi Colleges and Universities Key Laboratory of Applied Chemistry Technology and Resource Development, School of Chemistry and Chemical Engineering, Guangxi University, Nanning 530004, P. R. China

[b]Guangxi Key Laboratory of Petrochemical Resource Processing and Process Intensification Technology, Guangxi University, Nanning 530004, P. R. China

[*]Corresponding authors. E-mail: fanmg@gxu.edu.cn. and zjchen@gxu.edu.cn (Z. Chen)

Experimental Section

Chemicals and materials

Ni foam (≥99%, ~1.8 mm in thick) was purchased from Kunshan Jiayisheng Electronic Co., Ltd. Hydrochloric acid (HCl, 36–38%) was purchased from Chengdu Kelong Chemical Co., Ltd. Ethanol (C_2H_6O, 99.5%) and ethylene glycol ($C_2H_6O_2$, 99.5%) were purchased from Sichuan Xilong Science Co., Ltd. Nickel chloride hexahydrate ($NiCl_2·6H_2O$, 98%) and cobalt chloride hexahydrate ($CoCl_2·6H_2O$, 98%) were purchased from Guangdong Guanghua Sci-Tech Co., Ltd. Ammonium metavanadate (NH_4VO_3, 99%) was purchased from Tianjin Guangfu Technology Development Co., Ltd. All the chemicals were used as received without further purification.

Preparation of the NiCo/V_2O_3/C Catalyst

The NiCo/V2O3/C catalyst was prepared by solvothermal and thermal reduction processes. Firstly, a piece of NF with area of 1.5 cm × 4 cm was ultrasonically cleaned in 3 M hydrochloric acid solution (HCl), ethanol and deionized (DI) water for 15 min each. Secondly, 1 mmol $NiCl_2 \cdot 6H_2O$, 1 mmol $CoCl_2 \cdot 6H_2O$ and 2 mmol NH_4VO_3 were dissolved in a mixed solution of 20 ml DI water and 20 ml ethylene glycol (EG) and then transferred into a Teflon lined stainless autoclave with clean NF. Then keep the sealed autoclave at 180 °C for 12h. The product after reaction was washed several times with DI water and dried overnight at 60 °C to get the hydrothermal precursor. Finally, the hydrothermal precursor was thermally reduced at 400 °C in an Ar/H_2 atmosphere for 2 h under to obtain the target sample.

Preparation of Other Contrast Catalysts

For comparison, the preparation of the NiCo/C and V_2O_3/C catalysts were similar to the above method. The preparation of NiCo/C catalyst is to disperse $NiCl_2 \cdot 6H_2O$ and $CoCl_2 \cdot 6H_2O$ in the mixed solution during the above preparation process, while V2O3/C catalyst is to add only NH_4VO_3.

The Pt/C catalyst was prepared by the different method. Firstly, 5 mg of platinum/carbon (Pt/C, 20 wt% Pt on Johnson Matthey HISPEC3000) was ultrasonically dispersed in the mixed solution of 700 μL water, 300 μL isopropyl alcohol ($(CH_3)_2CHOH$, 99.7%, Shanghai Shenbo Chemical Co., Ltd) and 80 μL Nafion solution. Then, 5 μL of the catalyst ink was drop casted on the glassy-carbon electrode (0.07 cm^2).

Materials Characterization

The phase structure of the synthesized samples was analyzed by X-ray diffraction (XRD, Rigaku D/MAX-2500, Cu K_α radiation). Field-emission scanning electron microscope (FE-SEM, Thermo Fisher Scientific FEI Quattro S) and transmission electron microscope (TEM, FEI Talos F200S) were used to determine the morphology and composition of the samples. The synthesized samples were also characterized by Raman microscope (Renishaw, Horiba HR Evolution-800) and The X-ray photoelectron spectroscopy (XPS, Thermo Scientific ESCALAB 250Xi). The XPS peak positions were calibrated to the C 1s line (at 284.6 eV) of adventitious

hydrocarbon.

Electrochemical Measurements

All the electrochemical measurements were performed by the CHI 660E electrochemical analyzer (CH Instruments, Chenhua Co., Shanghai, China) and CS350M Electrochemical Workstation (Zhenming Scientific Instrument Co., Ltd. Wuhan, China) in a standard three-electrode system. The NF-supported catalysts were directly used as working electrode, the graphite rod was used as counter electrode, and the Hg/HgO electrode (with 1.0 M KOH) was used as reference electrode. All the potentials reported in our manuscript were converted to the reversible hydrogen electrode (RHE) scale according to the equation:

$E(\mathrm{RHE}) = E(\mathrm{Hg/HgO}) + 0.924$ V.

The polarization curves were recorded using linear sweep voltammetry (LSV) method by scanning the potential at a scan rate of 2 mV s^{-1}. Chrono potentiometric (CP) method at different target current densities was carried out to measure the long-term stability. Cyclic voltammetry (CV) cycles at the scan rate of 100 mV s^{-1} were performed to investigated another electrochemical stability test. All the potentials were manually corrected with 90% level iR compensation. The electrochemical impedance spectroscopy (EIS) was conducted using the CHI660E (CH Instruments, Inc.) electrochemical workstation, at overpotential of 10 mA cm^{-2} in a frequency range from 0.1 MHz to 0.1 Hz with an AC amplitude of 5 mV. The double-layer capacitance (C_{dl}) with CV method was measured to estimate the electrochemically active surface area (ECSA). The specific activity of catalysts was normalized by their ECSA, and the ECSA was calculated by the following equation:

$$\mathrm{ECSA} = C_{dl} / C_s \quad (1)$$

where C_{dl} is the double layer capacitance, and C_s is the specific capacitance.

Density functional theory (DFT) calculations

All the Density Functional Theory (DFT) calculations were performed using Vienna Ab initio Simulation Package (VASP) with the projector augmented wave (PAW) method. The Perdew-Burke-Ernzerhof (PBE) parameterization of the generalized

gradient approximation (GGA) is adopted to describe the exchange and correlation potential. During the geometry optimization and electronic structure calculations, the cut-off energy of the plane-wave basis set is 400 eV, and single gamma-point grid sampling was used for Brillouin zone integration. Atomic positions were optimized until the forces were less than 0.05 eV/Å. The first Brillouin zone was sampled by 1 × 1 × 1 k-mesh and a vacuum thickness of over 15 Å between periodic images was adopted, which was found to be sufficient for accurate results. Grimme's method (DFT-D3) was carried out to include explicit dispersion correction terms to the energy.

The work functions of NiCo (111), V_2O_3 (001), and NiCo/V_2O_3 Mott-Schottky heterojunction were calculated to study the origin of electron transfer. According to the current theories, the work function (Φ) is the minimum energy required for an electron to escape from the Fermi level to the vacuum level, it can be expressed as the following equation:

$$\Phi = E(\text{Vacuum}) - E(\text{Fermi}) \quad (2)$$

where E(Vacuum) and E(Fermi) are the electrostatic potentials of vacuum energy level and Fermi energy level, respectively.

The calculation of CDD at NiCo/V_2O_3 can be presented as the following equation:

$$\rho = \rho(\text{NiCo/V2O3}) - \rho(\text{NiCo}) - \rho(\text{V2O3}) \quad (3)$$

where ρ(NiCo/V_2O_3), ρ(NiCo) and ρ(V_2O_3) represent the charge density of the corresponding geometries.

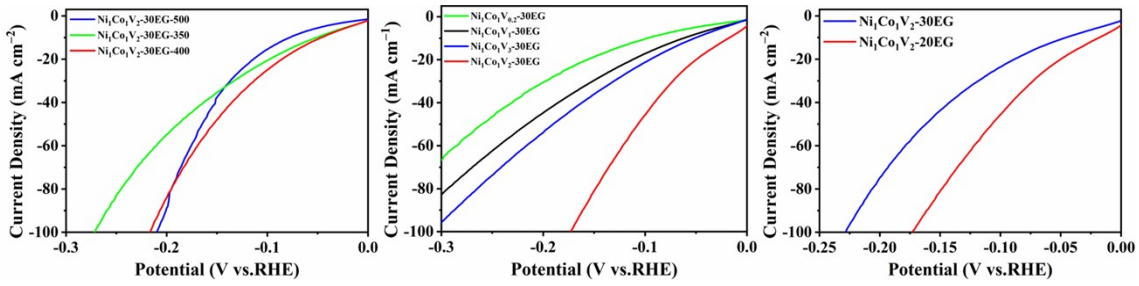

Figure S1. HER polarization curves of hydrothermal precursor samples with various annealing temperatures, amounts of NH_4VO_3 and volumes of ethylene glycol during

the annealing process.

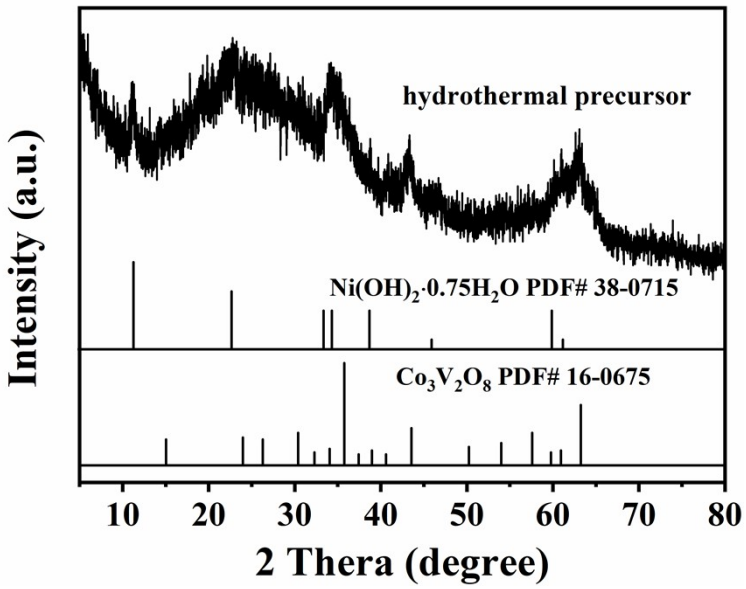

Figure S2. XRD result of the hydrothermal precursor sample.

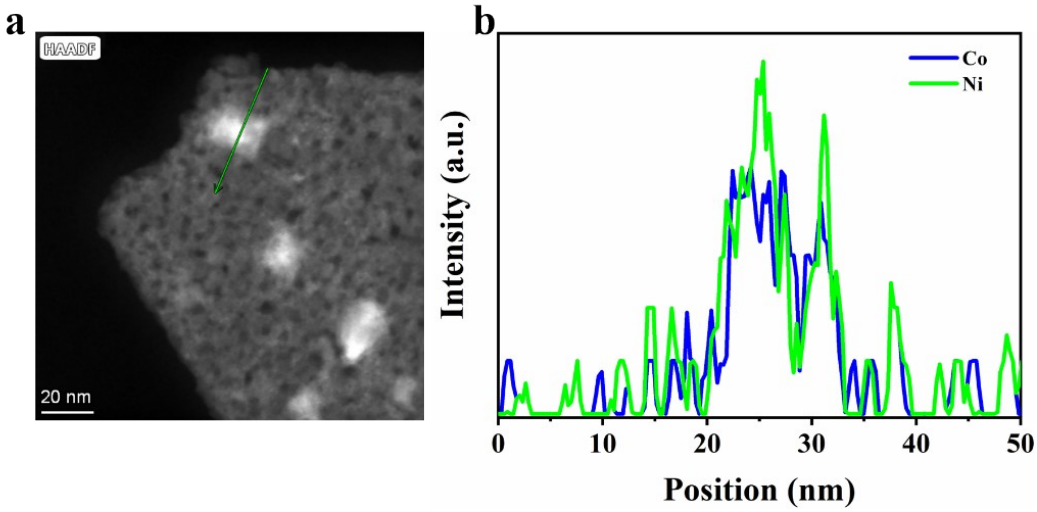

Figure S3. a) EDS line scan and b) corresponding Ni,Co dispersion of $NiCo/V_2O_3/C$ sample.

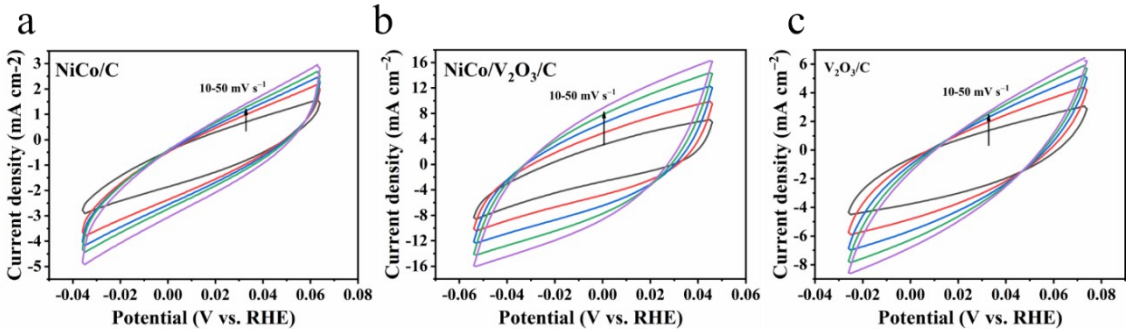

Figure S4. Cyclic voltammogram profiles of the $NiCo/V_2O_3/C$ sample and contrat samples at different scan rates

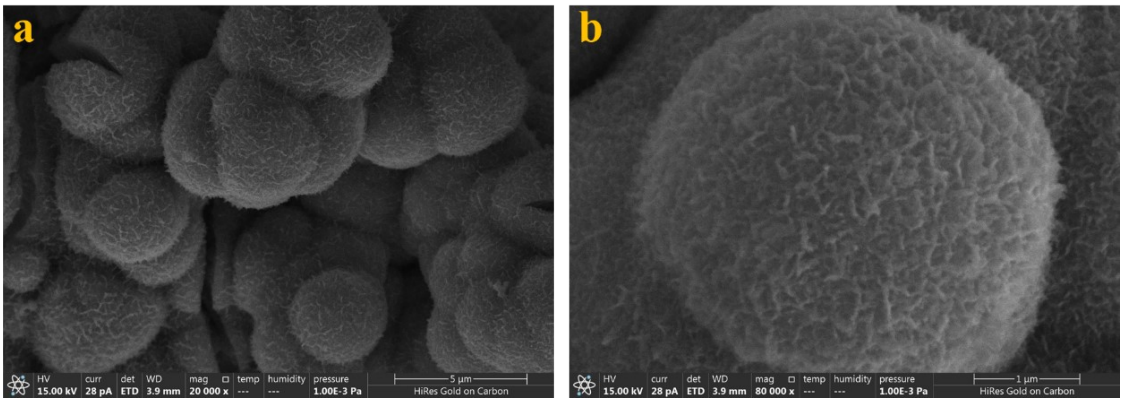

Figure S5. SEM images of the $NiCo/V_2O_3/C$ sample after HER stability test.

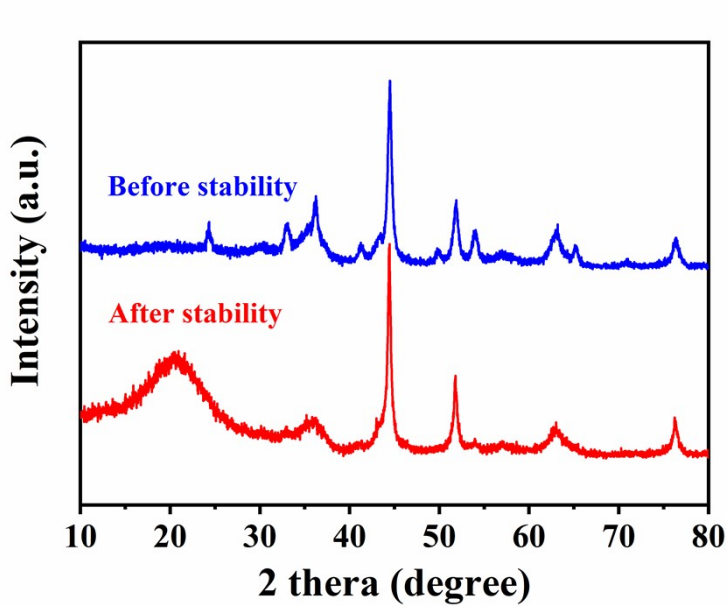

Figure S6. XRD result of the he $NiCo/V_2O_3/C$ sample after stability test.

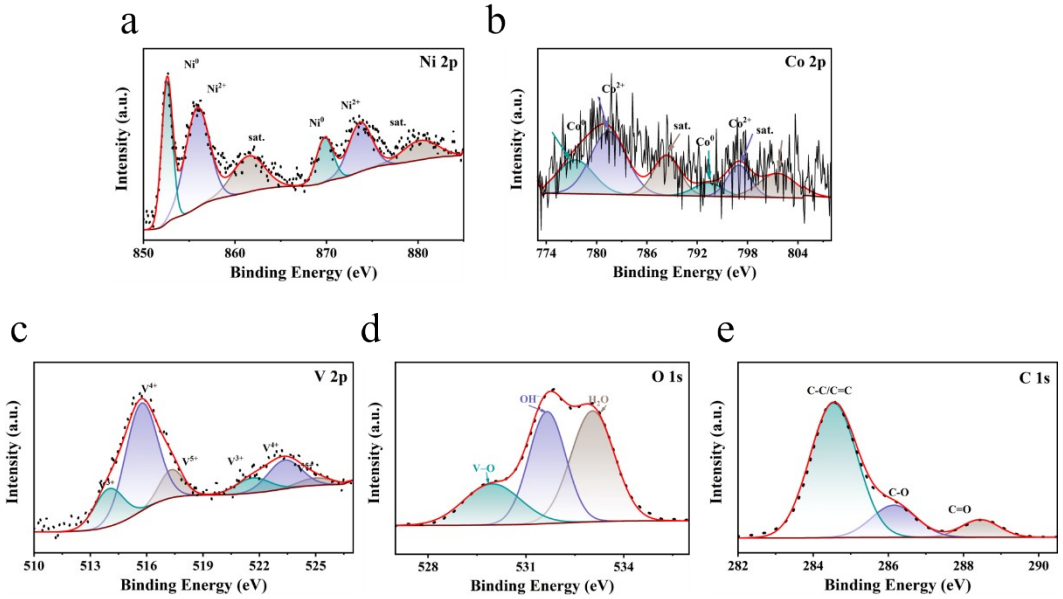

Figure S7. (a) Ni 2p and (b) Co 2p, (c) V 2p, (d) O 1s (e) C 1sXPS spectra of the $NiCo/V_2O_3/C$ sample after stability test.

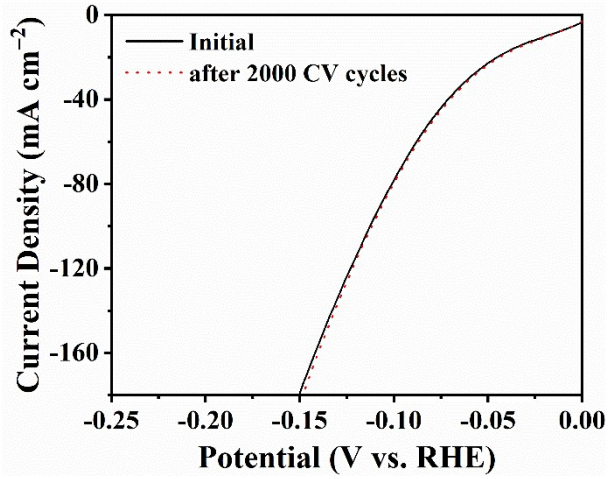

Figure. S8. Comparison of HER polarization curves of $NiCo/V_2O_3/C$ catalyst before and after 2000 CV cycles.

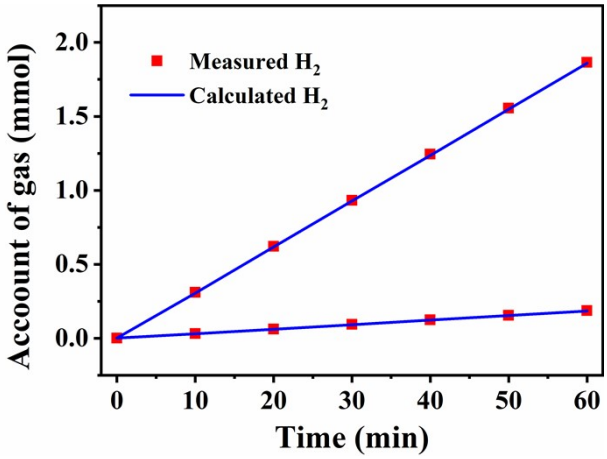

Figure S9. Faradaic efficiency and practical measured amount of H_2 product vs. theoretically calculated quantities at 10 mA cm^{-2} and 100 mA cm^{-2}.

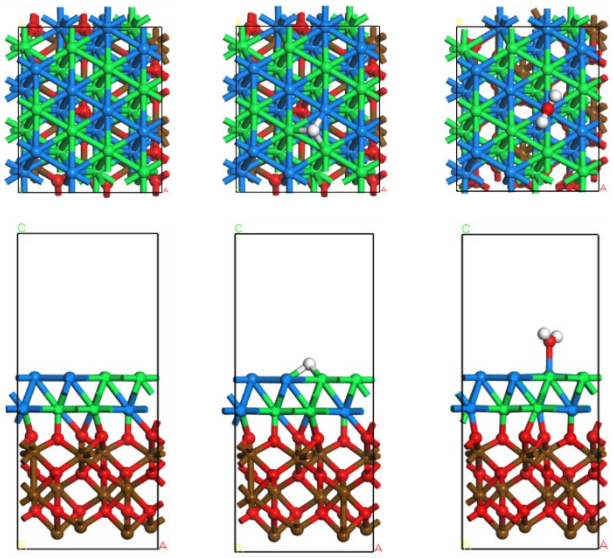

Fig. S10 Calculated geometries of (a) clean, (b) hydrogen adsorbed, (c) H_2O adsorbed on $NiCo/V_2O_3$ surface. Green, blue, brown, red, and white spheres in geometries represent the Ni, Co, V, O, and H atoms, respectively.

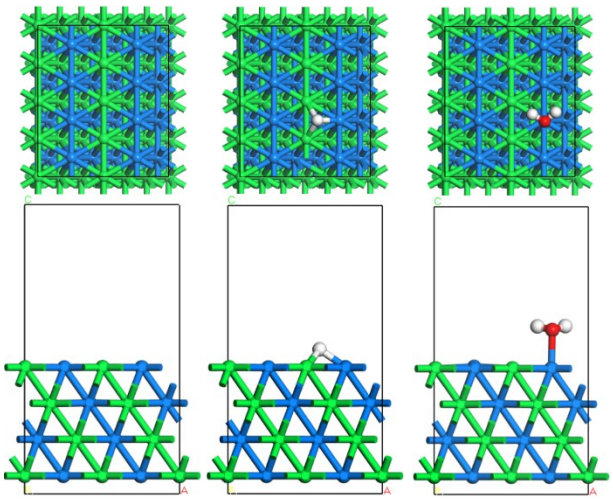

Fig. S11 Calculated geometries of (a) clean, (b) hydrogen adsorbed, (c) H_2O adsorbed on NiCo alloy surface. Green, blue, red, and white spheres in geometries represent the Ni, Co, O, and H atoms, respectively.

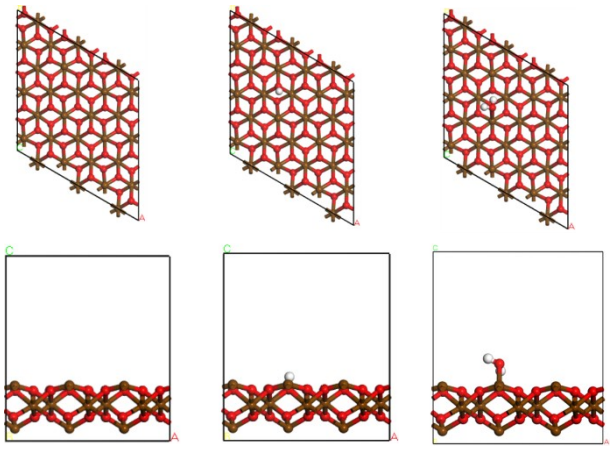

Fig. S12 Calculated geometries of (a) clean, (b) hydrogen adsorbed, (c) H_2O adsorbed on V_2O_3 surface. Brown, red, and white spheres in geometries represent the V, O, and H atoms, respectively.

Table S1. Summary of HER performance of recently reported catalysts in literature.

Catalyst	Electrolyte	Current density (mA cm^{-2})	Overpotential (mV)	Ref.
W-NiCo	1.0 M KOH	10	192	[1]
Mo_2N /CeO_2@NF	1.0 M KOH	10	26	[2]
CuCo@NC	1.0 M KOH	10	163	[3]
Ni_3N-V_2O_3-1-1/NF	1.0 M KOH	10	40	[4]
Ni_4Mo-V_2O_3	1.0 M KOH	10	39.3	[5]
TMP NiZn-Ni/NF	1.0 M KOH	600	233	[6]
NiCo@C-NiCoMoO/NF	1.0 M KOH	10	39	[7]
	1.0 M KOH	1000	266	
NiCoFe-NDA	1.0 M KOH	10	215	[8]
	1.0 M KOH	325	1800	
CrO_x/Cu–Ni/Cu foam	pH 7 buffer electrolyte	10	48	[9]
V_2O_3/Ni/NF	1.0 M KOH	10	54	[10]
NiCo@N,P-CNSs	1.0 M KOH	10	99	[11]
Ni/CeO_2@N-CNFs	1.0 M KOH	10	100	[12]
V-CoP	1.0 M KOH	10	46	[13]
Ni_3N-VN	1.0 M KOH	10	37	[14]
A-NiCo LDH/NF	1.0 M KOH	100	151	[15]
	1.0 M KOH	500	286	
	1.0 M KOH	1000	381	
Cu@CoFe	1.0 M KOH	10	171	[16]
$NiCoS_x$@CoCH NAs/NF	1.0 M KOH	1000	438	[17]
NiCo/V_2O_3/C/NF	1.0 M KOH	10	23	This work
	1.0 M KOH	1000	396	This work

Reference:

1.D. Gao, J. Guo, H. He, P. Xiao and Y. Zhang, *Chem. Eng. J.*, 2022, **430**, 133110.

2.C. Wang, X. Lv, P. Zhou, X. Liang, Z. Wang, Y. Liu, P. Wang, Z. Zheng, Y. Dai, Y. Li, M. H. Whangbo and B. Huang, *ACS Appl. Mater. Interfaces*, 2020, **12**, 29153-29161.

3.M. Kuang, Q. Wang, P. Han and G. Zheng, *Adv. Energy Mater.*, 2017, **7**, 1700193-1700200.

4.P. Zhou, G. Zhai, X. Lv, Y. Liu, Z. Wang, P. Wang, Z. Zheng, H. Cheng, Y. Dai and B. Huang, *Appl. Catal. B*, 2021, **283**, 119590.

5.Z. Xie, W. Wang, D. Ding, Y. Zou, Y. Cui, L. Xu and J. Jiang, *J. Mater. Chem. A*, 2020, **8**, 12169-12176.

6.Q. Zhou, Q. Hao, Y. Li, J. Yu, C. Xu, H. Liu and S. Yan, *Nano Energy*, 2021, **89**, 106402.

7.G. Qian, J. Chen, T. Yu, L. Luo and S. Yin, *Nanomicro Lett*, 2021, **13**, 77.

8.B. Y. Xia, Y. Yan, X. Wang, Y. Kong, J. Zhang, P. Wang, C. Xia, Y. Zhu, J. Liu and K. Yue, *Energy Environ. Sci.*, 2021, **14**, 6546-6553.

9.C.-T. Dinh, A. Jain, F. P. G. de Arquer, P. De Luna, J. Li, N. Wang, X. Zheng, J. Cai, B. Z. Gregory, O. Voznyy, B. Zhang, M. Liu, D. Sinton, E. J. Crumlin and E. H. Sargent, *Nat. Energy*, 2018, **4**, 107-114.

10.Q. Zhang, B. Liu, L. Li, Y. Ji, C. Wang, L. Zhang and Z. Su, *Small*, 2021, **17**, 2005769-2005778.

11.T. Li, G. Luo, Q. Liu, S. Li, Y. Zhang, L. Xu, Y. Tang, J. Yang and H. Pang, *Chem. Eng. J.*, 2021, **410**, 128325.

12.T. Li, J. Yin, D. Sun, M. Zhang, H. Pang, L. Xu, Y. Zhang, J. Yang, Y. Tang and J. Xue, *Small*, 2022, **18**, 2106592 -2106601

13.R. Zhang, Z. Wei, G. Ye, G. Chen, J. Miao, X. Zhou, X. Zhu, X. Cao and X. Sun, *Adv. Energy Mater.*, 2021, **11**, 2101758-2101768.

14.H. Yan, Y. Xie, A. Wu, Z. Cai, L. Wang, C. Tian, X. Zhang and H. Fu, *Adv. Mater.*, 2019, **31**, 1901174- 1901182.

15.H. Yang, Z. Chen, P. Guo, B. Fei and R. Wu, *Appl. Catal. B*, 2020, **261**, 118240.

16.L. Yu, H. Zhou, J. Sun, F. Qin, D. Luo, L. Xie, F. Yu, J. Bao, Y. Li, Y. Yu, S. Chen and Z. Ren, *Nano Energy*, 2017, **41**, 327-336.

17.X. Zhang, R. Zheng, M. Jin, R. Shi, Z. Ai, A. Amini, Q. Lian, C. Cheng and S. Song, *ACS Appl. Mater. Interfaces*, 2021, **13**, 35647-35656.